Rise and fall time behavior of the gyrotron backward-wave oscillator

K. F. Pao,[1] T. H. Chang,[2] S. H. Chen,[3] and K. R. Chu[2]
[1]*Physics Division, National Center for Theoretical Sciences, Hsinchu, Taiwan*
[2]*Department of Physics, National Tsing Hua University, Hsinchu 300, Taiwan*
[3]*Department of Physics, National Changhua University of Education, Changhua, Taiwan*
(Received 2 June 2006; published 16 October 2006)

The rise and fall time behavior of a pulsed microwave oscillator is a problem of academic interest. It is also of importance to radar and other applications because it can lead to phase and frequency jitters or even lock the entire pulse into an undesired mode. Here we present a study of the rise and fall time behavior in the gyrotron backward-wave oscillator (gyro-BWO). Single-mode simulations reveal that, during the rise and fall portions of the electron beam pulse, oscillation frequencies of the axial modes vary in such a way that their transit angles remain at the respective optimum values. Thus, axial mode competition and mode switching can readily take place in these transient stages. Time-dependent simulations demonstrate that, under both the gradual and instant turn-on conditions, the axial modes compete in a pattern governed by the characteristic asymmetry of the mode profiles. Other aspects of physics interest include the analysis and explanation of a resultant hysteresis effect between the rise and fall portions of the beam pulse. These understandings are expected to provide the basis for achieving a stable gyro-BWO operating at a single mode throughout the entire beam pulse.

DOI: 10.1103/PhysRevE.74.046405 PACS number(s): 84.40.Ik, 84.40.Fe

I. INTRODUCTION

The voltage and current of a pulsed electron beam depart considerably from the design values in the rise and fall stages of the beam pulse. Consequently, different modes can be excited in sequence or simultaneously during these transient periods, causing pulse-to-pulse phase and frequency jitters of the microwave pulse [1,2]. In some cases, an oscillator can be locked into an early starting, undesired mode even when the beam pulse flattens. This is an issue of practical as well as academic interest and has been studied in theory [3–6] and in experiment [7] for the gyromonotron, the most mature version of gyrodevices driven by the electron cyclotron maser instability [8,9]. For the resonator-based gyromonotron, the oscillation frequency is largely fixed by the resonator structure. Voltage and pitch-angle variations of the electron beam during the rise and fall portions of the pulse consequently result in transit angle variations for a number of modes, and each of these modes can be excited over a duration in which its transit angle transitions through the optimum value ($\sim\pi$). Mode competition and mode control of the gyromonotron have been considered under different detuning conditions and cathode/anode voltage profiles during the rise time [3,4]. As a rule [5,7], especially when there is sufficient time for the competing modes to build up during the voltage rise, one must find a start-up scenario in which the desired mode has the lowest oscillation threshold so that it is excited before the unwanted modes. The underlying physics is that the existing mode tends to suppress the growth of other modes.

By comparison, the rise and fall time behavior of the gyrotron backward-wave oscillator (gyro-BWO) has received very little, if any, attention partly because of the less developed status of this class of continuously tunable gyrodevices. On the other hand, a radically different picture of mode competition has been reported in a recent study [10]. It is shown that the asymmetry of the gyro-BWO axial field profile, rather than the start-oscillation current, determines the competitiveness of a specific mode. As a result, a fast-growing and well-established mode will subsequently be suppressed by a later-starting mode with a more favorable field profile. This is expected to have important implications on the rise and fall time behavior of the gyro-BWO. Moreover, the gyro-BWO oscillations build up in an *internal* feedback loop, rather than the reflective feedback loop as in the gyromonotron. The loop is formed of a forward moving electron beam and backward propagating waves of a waveguide mode (Fig. 1). In the absence of end reflections, there are no cold resonant modes. The oscillation frequency is free to assume any value over a continuous range, and identities of the axial modes are determined entirely by the electron dynamics rather than by the interaction structure. As a result, it has been shown [11] that the (hot) axial modes are linearly characterized by a discrete set of optimum transit angles Θ separated by $\sim 2\pi$. This is also expected to affect the rise and fall time behavior in a significant manner.

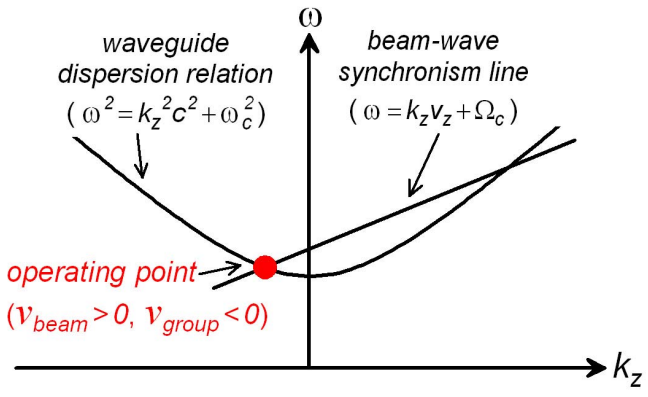

FIG. 1. (Color online) ω-k_z diagram showing the waveguide mode, the beam-wave synchronism line, and the operating point of the gyro-BWO.

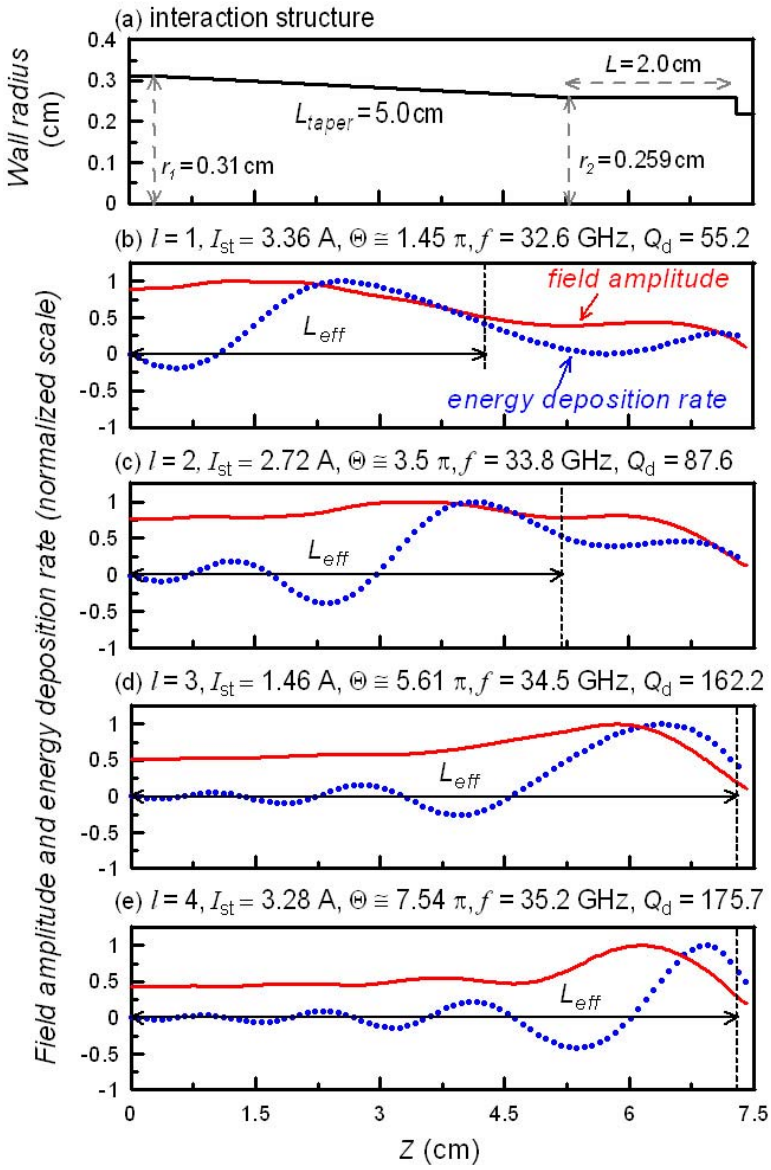

FIG. 2. (Color online) (a) Configuration and dimensions of the gyro-BWO interaction structure under study. (b)–(e) Field amplitudes (lines) and beam energy deposition rates (dots) vs z for the first four axial modes at their respective I_{st} values. V_b=95 kV, $v_\perp/v_z$=1.1, r_c (guiding center position) =0.09 cm, $\Delta v_z/v_z$ (axial velocity spread) =5%, and B_0=14.8 kG (=1.32 times the left-end grazing field and 1.1 times the right-end grazing field).

Motivated by these considerations, here we present a follow-up study (in particular to Ref. [10]) which focuses on the rise and fall time behavior of the gyro-BWO. In Sec. II, we begin with a review of the steady-state characteristics of the gyro-BWO axial modes. These modes are distinguished by their different transit angles and field profiles in a way fundamentally different from the gyromonotron. Axial modes are next characterized in the rise and fall stages of the beam pulse. The constancy of their characteristic transit angles (in spite of a large variation of the beam voltage) suggests that multiple axial modes can be excited at any given instant when the beam voltage and current rise above their thresholds. In Sec. III, evolution of these axial modes during the voltage rise and fall is followed by time-dependent simulations and compared with that under the instant turn-on condition. The pattern and governing mechanism for the competition are found to be the same through a time-frequency analysis of the output signals. In both cases, the oscillation is eventually dominated by the lowest order mode with the most favorable field profile. A distinctive hysteresis effect, exhibited between the rise and fall portions of the beam pulse, is also studied in Sec. III. In Sec. IV, we present a brief conclusion.

II. LINEAR THEORY OF THE AXIAL MODES

A single-mode stationary code [12] has been employed for the investigation of individual mode properties. The transverse field profile is assumed to be that of an unloaded waveguide, while the axial field profile is self-consistently evaluated by imposing outgoing and evanescent wave boundary conditions at the upstream and downstream ends, respectively. The specific configuration under study is a TE_{11}-mode gyro-BWO operating in the Ka-band [Fig. 2(a)]. It consists of a slightly down-tapered waveguide and a short uniform section, and is terminated in the downstream end with a cutoff section. The down-tapered structure is chosen because it has the effect of significantly enhancing the interaction efficiency [13].

A. Steady-state characteristics of axial modes

The linear field amplitudes (solid curves) and beam-energy deposition profiles (dots) of the first four axial modes ($l=1-4$) at their respective I_{st} values are displayed in Figs. 2(b)–2(e) with relevant parameters given in the figure and figure caption (I_{st} for the $l>4$ modes are above the maximum beam current under study). Regions to the right of vertical dashed lines are cutoff to the oscillation frequency. Thus, we may define an effective interaction length, L_{eff}, as the length to the left of the vertical lines. Consistent with [10,11], the (hot) axial modes are seen to be characterized by a discrete set of optimum (linear) transit angles (Θ) separated by $\sim 2\pi$, where Θ is the total wave phase variation experienced by the electron in traversing the effective interaction space. For the fundamental cyclotron harmonic interaction, Θ is defined as

$$\Theta = (\omega - k_z v_z - \Omega_c)\frac{L_{eff}}{v_z}, \tag{1}$$

where ω is the wave frequency, k_z is the cold propagating constant (a negative value for backward wave interactions), v_z is the initial electron axial velocity, and Ω_c is the initial relativistic electron cyclotron frequency.

It can be seen in Fig. 2 that the field amplitude always begins with an initial absorption dip [8]. Each increase in the mode index is accompanied with a step increase in Θ ($\sim 2\pi$), which brings Θ to the next optimum value. This hence results in one more region of beam-energy absorption and an additional trough of the field amplitude. The difference in energy deposition profiles thus gives each axial mode a distinctive asymmetry in field distribution. A lower (higher) order mode has a field peak closer to (further away from) the beam entrance. The proximity of the field peak to the beam entrance therefore affords the lower order mode the advantage of early interaction with the electron beam.

For later interpretation of the multimode simulation data, it is useful to calculate the diffraction quality factor (Q_d) for each mode. Q_d is defined as

$$Q_d = \frac{\omega W_f}{P_{out}}, \tag{2}$$

where P_{out} is the output power from the upstream end and W_f is the total field energy within the effective length. Because the Ohmic loss amounts to less than one percent of the output power, Q_d is essentially the total Q. The calculated Q_d is 55.2, 87.6, 162.2, and 175.7 for $l=1$, 2, 3, and 4, respectively. A higher order mode has a higher Q_d value because it has a longer L_{eff} and its field strength (hence power flow) is weaker at the output end. As will be shown later, a higher order mode will grow at a faster rate given the same excitation power.

Figure 3 displays the I_{st} and oscillation frequency as a function of the applied magnetic field B_0 for the $l=1-4$ modes. The diverse behavior of the I_{st} curves is caused by the interplay among three factors, all of which influence the

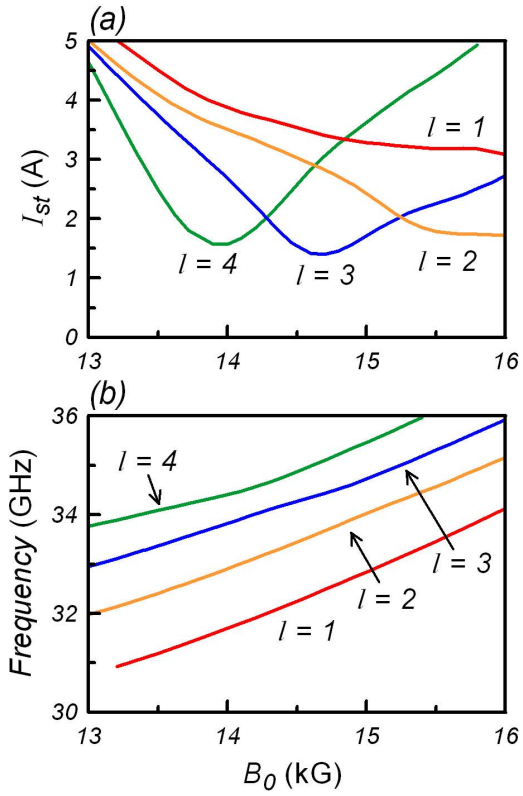

FIG. 3. (Color online) (a) Start-oscillation currents and (b) corresponding oscillation frequencies vs B_0 for the first four axial modes. Beam parameters are the same as in Fig. 2.

I_{st} value: (1) a longer L_{eff} tends to lower the I_{st}; (2) a larger Θ (implying weaker interaction strength) tends to raise the I_{st}; and (3) a higher oscillation frequency (hence higher k_z) tends to raise the I_{st} because of the greater axial debunching forces at a larger k_z [14]. The first factor plays the dominant role at lower magnetic fields where different modes penetrate at different depths (L_{eff}) into the tapered section. Thus, a higher order mode with a higher oscillation frequency and deeper penetration depth has a lower I_{st}. However, this advantage for a given mode disappears as B_0 (hence the oscillation frequency) increases to the value for which the fields of this mode extend to the full length of the physical structure. Any further increase in B_0 brings up the wave number k_z, but no longer L_{eff}. As a result, I_{st} of this mode starts to rise because of the increased debunching forces [e.g., the $l=3-4$ modes in Fig. 3(a)], while I_{st} of the lower order modes continues to fall upon further increases in their L_{eff} [e.g., the $l=1-2$ modes in Fig. 3(a)]. For modes with the same L_{eff}, such as the $l=3-4$ modes at $B_0=14.8$ kG [Figs. 2(d) and 2(e)], factor (1) no longer plays a role and factors (2) and (3) both predict a higher I_{st} for a higher order mode (a reversal from the low magnetic field case), as is evident in Fig. 3(a).

B. Rise and fall time characteristics of axial modes

Because the gyro-BWO employs a nonresonant interaction structure, the electron beam is capable of exerting a much stronger effect on the oscillation frequency as com-

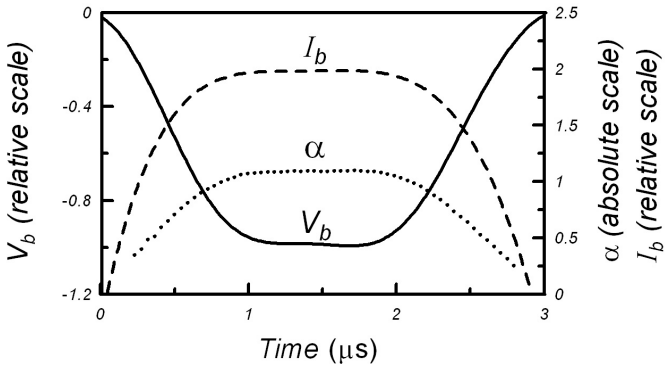

FIG. 4. Temporal profiles of the beam voltage (V_b, solid line), current (I_b, dashed line), and perpendicular-to-parallel velocity ratio (α, dots) used for the simulation.

pared with the resonator-based oscillators. Such effects are expected to be even more strongly exhibited during the voltage rise and fall. In this section, we examine the significance of frequency variations on the single-mode behavior for a typical beam pulse shown in Fig. 4.

Figure 5(a) shows the beam current (I_b, dashed line) and I_{st} (solid lines) of the first four axial modes as functions of V_b. Each intersection of I_b and I_{st} signals the start of an axial mode during the voltage rise or its disappearance during the voltage fall, in accordance with the single-mode theory. Figure 5(b) displays the characteristics of different axial modes.

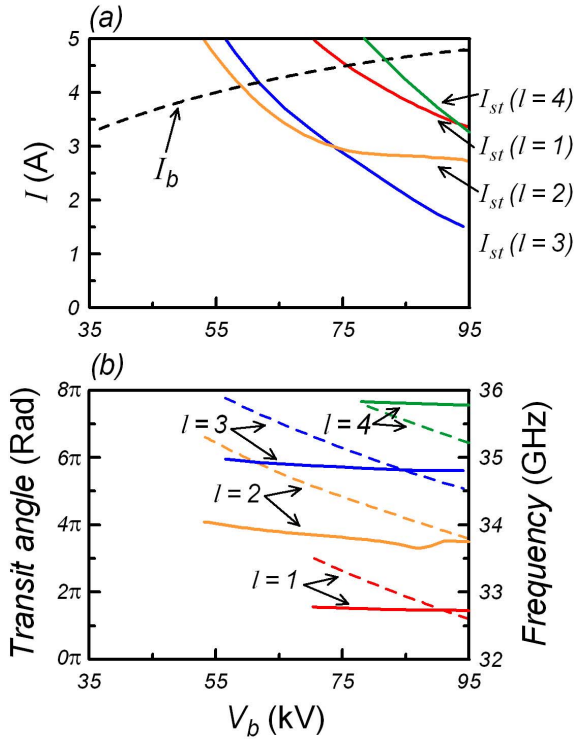

FIG. 5. (Color online) (a) Beam current (dashed line) and start-oscillation currents (solid lines) vs V_b for the first four axial modes up to the peak beam voltage of 95 kV. (b) The corresponding oscillation frequencies (dashed lines) and electron transit angles (Θ, solid lines) vs V_b. The beam α value as a function of V_b is shown in Fig. 4. Other operating parameters are the same as in Fig. 2.

The oscillation frequency varies with the beam voltage as expected. However, it varies in such a way so that the transit angle of a given mode remains at a nearly-constant optimum value. This explains why I_{st} values of the axial modes all fall monotonically as the voltage increases [Fig. 5(a)] and also suggests the possibility of multimode excitation during the voltage rise and fall.

III. MULTIMODE BEHAVIOR

In a recent publication [10], we studied axial mode competition in the gyro-BWO with emphasis on the physical mechanism, asymmetry of field profiles, which governs the competition. Here, relevant results in that study [Figs. 6(b) and 6(e)] will be presented as background information for a follow-up study on an interesting hysteresis effect and a comparative study of the instant turn-on model.

A. Mode competition during the voltage rise and fall

Figure 6 displays a typical three-mode competition/switching sequence obtained with a time dependent, particle-in-cell code [10] over the entire duration of the beam pulse shown in Fig. 6(a). Multimode behavior in the competition process, embedded in the output signal [Fig. 6(b)], is resolved with a time-frequency analysis [15,16] and displayed in Figs. 6(c)–6(e). In Fig. 6(d), it is seen that a higher order axial mode has a higher linear growth rate because it has a higher Q_d value (Fig. 2). As expected from the order of intersections of the I_b curve with the I_{st} curves in Fig. 5(a), the $l=2$ mode is excited slightly ahead of the $l=3$ mode. However, the $l=3$ mode immediately becomes the dominant mode [Figs. 6(d) and 6(e)] because it grows linearly at a greater rate than the $l=2$ mode. In the ensuing nonlinear stage, the $l=3$ mode, in spite of its large amplitude, is rapidly suppressed by the slowly-growing $l=2$ mode, which has a more favorable field profile. As the beam current rises above the threshold of the $l=1$ mode, the $l=2$ mode is in turn suppressed by the $l=1$ mode, which has the most favorable field profile. In the presence of the large-amplitude $l=1$ mode, the $l=4$ mode never has a chance to be excited and the $l=1$ mode remains the sole stationary mode over the flat portion of the beam pulse. The finite line width of the mode spectrum in Fig. 6(e) is due to the short time window (8 nsec) employed in the time-frequency analysis.

In the fall portion of the beam pulse, the $l=1$ mode starts to decay away as I_b falls toward (and eventually below) its threshold current. This triggers a new round of mode competition. The $l=3$ mode with the largest growth rate re-emerges first and is subsequently suppressed by the $l=2$ mode [Fig. 6(c)] in the same manner as during the rise time. We note also that, consistent with the predictions of Fig. 5(b), the oscillation frequency is higher at a lower beam voltage. This is an indirect verification of the constancy of the transit angles shown in Fig. 5(b).

B. A hysteresis effect and its physical interpretation

In Fig. 6(c), the asymmetric order of appearance of the dominant mode; namely, $l=3\rightarrow2\rightarrow1\rightarrow3\rightarrow2$, indicates a

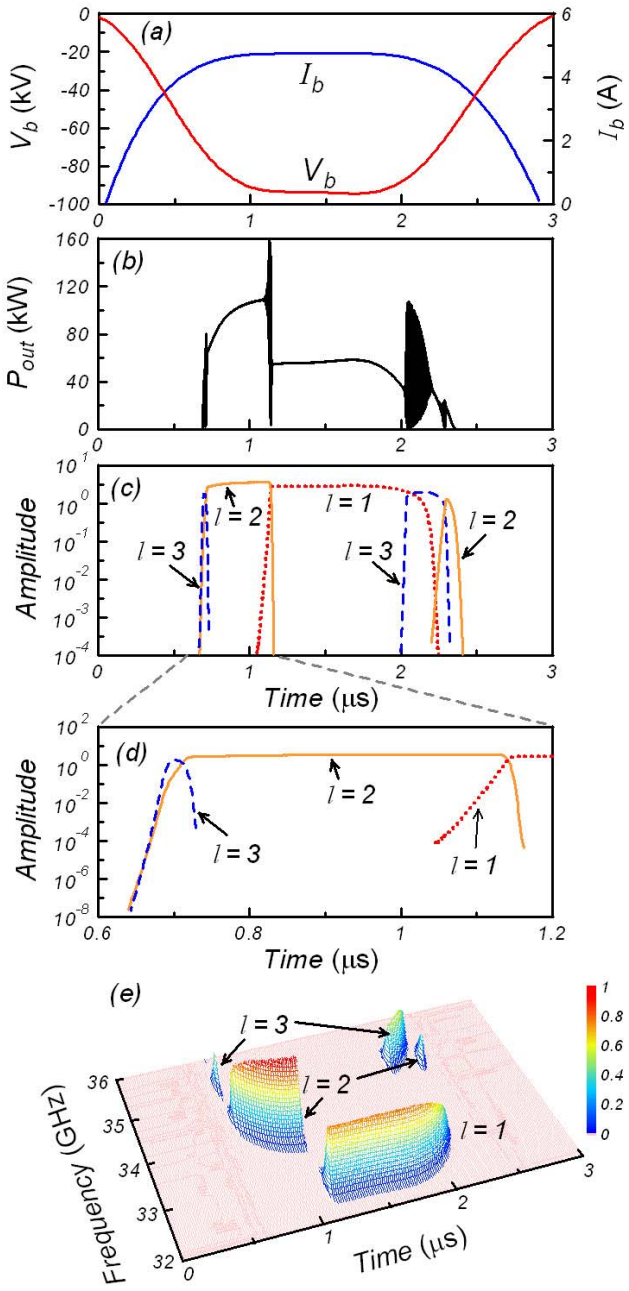

FIG. 6. (Color online) (a) Temporal profiles of the beam voltage and current (reproduced from Fig. 4) used in the simulation. Other parameters are the same as in Fig. 2. (b) Simulated output power (P_{out}) vs time. (c) Temporal evolution of axial modes over the entire beam pulse. (d) A close-up view of (c) from $t=0.6$ μs to $t=1.2$ μs. (e) Time-dependent spectrum of the output signal (amplitude in color code).

hysteresis effect between the rise and fall times. This can be attributed to the optimum transit angles maintained by all of the axial modes throughout the beam pulse. These axial modes remain competitive as long as the beam current is above their thresholds. Thus, the highest order mode in the competition (the $l=3$ mode) rapidly grows to the dominant stage before it is suppressed by the $l=2$ mode. This explains why the $l=3$ mode always precedes the $l=2$ mode in both the rise and fall stages.

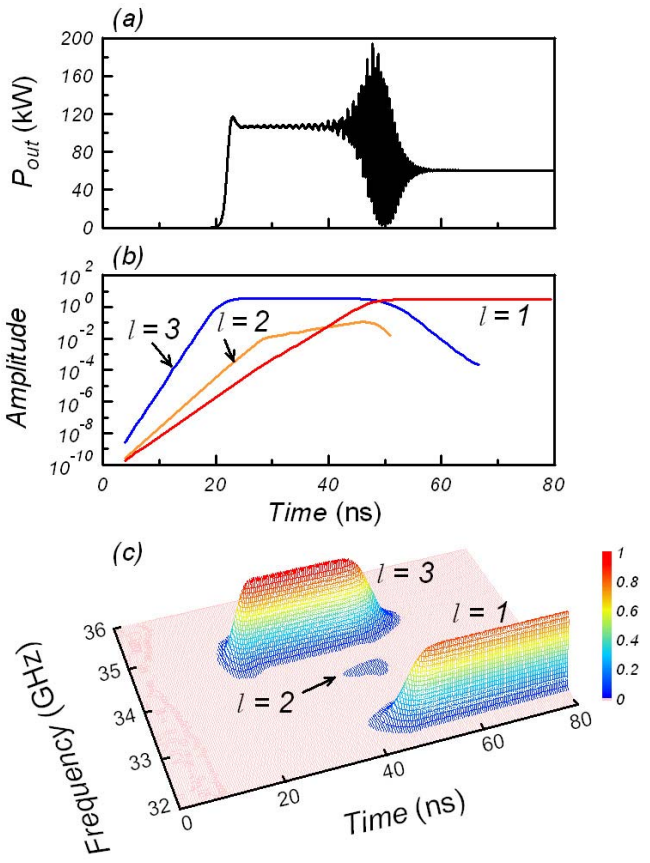

FIG. 7. (Color online) (a) Simulated output power (P_{out}) vs time for an instant turn-on model. $I_b=4.8$ A and other parameters are the same as in Fig. 2. (b) Temporal evolution of the axial modes. (c) Time-dependent spectrum of the output signal (amplitude in color code).

In Ref. [10], an experimental study with the same configuration and beam parameters (including the voltage/current profiles) was reported. Except for minor quantitative differences, the experiment yielded essentially the same results as shown in Fig. 6, including the temporal traces of the output power, the time-dependent frequency spectrum, the time duration of mode competition, and the hysteresis effect on mode transitions.

By comparison, in the gyromonotron, the optimum condition ($\Theta \sim \pi$) for different modes appears in sequence, each for a fraction of the voltage rise (or fall) time, which is responsible for the mode hopping phenomenon often observed during the startup of the gyromonotron [3]. For the same reason, the return path during the fall time traces backward along the original path in terms of the order of mode excitation, although the mode duration and amplitude may not be identical to those during the rise time [17].

C. Instant turn-on scenario and time scale of mode competition

Since the mode competition process discussed so far occurs during the voltage rise and fall, questions arise as to whether the pattern and mechanism of mode competition shown in Fig. 6 are of a general nature or specific to the rise

and fall times. In addition, the relatively long rise and fall times (~ 1 μsec) have obscured the time scale of the competition process. To address these issues, we present below simulation results on an instant turn-on model with identical parameters as used for Fig. 6 except for the assumption of zero rise and fall times.

The multimode competition process for a beam turned on at full current (4.8 A) and full voltage (95 kV) is demonstrated in Fig. 7. Extrapolating the data in Fig. 7(b) to the onset of the beam pulse ($t=0$), the first three axial modes are observed to be excited simultaneously, whereas the $l=4$ mode, if present, is too weak to be diagnosed within the resolution of our time-frequency analysis. The pattern of mode competition is similar to that shown in Fig. 6; namely, the linear growth rate and the field asymmetry determine, respectively, the initially and eventually dominant mode in the competition. Thus, the evolution in Fig. 7 begins with the dominance of the $l=3$ mode and settles down at the $l=1$ mode. However, the oscillation frequency of each mode now stays at a constant value [Fig. 7(c)] because the beam voltage remains constant. The simultaneous excitation of the $l=1-3$ modes implies a reduced role for the $l=2$ mode, which has neither the highest growth rate nor the most favorable field profile. Figure 7 also shows a time scale of only 10–20 nsec for each mode competition process. This results in rapid mode switching as the beam voltage and current vary on a time scale of hundreds of nsec [see Fig. 6(e)].

IV. CONCLUSION

The rise and fall time behavior of the gyro-BWO has been studied in the perspective of beam-wave interaction dynamics. At a fixed magnetic field, the oscillation frequencies of axial modes vary with the beam voltage in a manner such that the transit angles remain at their respective optimum values. The constancy of optimum transit angles suggests the possibility of simultaneous, rather than sequential, excitation of the axial modes. The higher order mode gains a head start with a higher growth rate, while the lower order mode possesses a stronger competitive edge with a more favorable field profile. Consequently, the evolution is characterized by a sequence of mode switching, each occurring on a time scale of 10–20 nsec. This pattern of mode-mode interactions also leads to a hysteresis effect fundamentally different from that of resonator-based oscillators, in which different modes tend to be excited sequentially during the voltage rise and fall. In terms of practical applications, an in-depth understanding of the rise and fall time behavior provides the physics basis for achieving a gyro-BWO with minimum pulse-to-pulse phase and frequency jitters.

ACKNOWLEDGMENTS

This work was supported by the National Science Council, Taiwan. The authors are grateful to C. T. Fan, N. C. Luhmann, Jr., and L. R. Barnett for their critical comments.

[1] A. H. McCurdy, C. M. Armstrong, W. M. Bollen, R. K. Parker, and V. L. Granatstein, Phys. Rev. Lett. **57**, 2379 (1986).
[2] A. H. McCurdy and C. M. Armstrong, IEEE Trans. Microwave Theory Tech. **36**, 891 (1988).
[3] B. Levush and T. M. Antonsen, Jr., IEEE Trans. Plasma Sci. **18**, 260 (1990).
[4] D. R. Whaley, M. Q. Tran, T. M. Tran, and T. M. Antonsen, Jr., IEEE Trans. Plasma Sci. **22**, 850 (1994).
[5] G. S. Nusinovich, IEEE Trans. Plasma Sci. **27**, 313 (1999).
[6] G. S. Nusinovich, O. V. Sinitsyn, L. Velikovich, M. Yeddulla, T. M. Antonsen, Jr., A. N. Vlasov, S. R. Cauffman, and K. Felch, IEEE Trans. Plasma Sci. **32**, 841 (2004).
[7] K. E. Kreischer and R. J. Temkin, Phys. Rev. Lett. **59**, 547 (1987).
[8] K. R. Chu, Rev. Mod. Phys. **76**, 489 (2004).
[9] G. S. Nusinovich, *Introduction to the Physics of Gyrotrons* (Johns Hopkins University Press, Maryland, 2004).
[10] K. F. Pao, T. H. Chang, C. T. Fan, S. H. Chen, C. F. Yu, and K. R. Chu, Phys. Rev. Lett. **95**, 185101 (2005).
[11] S. H. Chen, T. H. Chang, K. F. Pao, C. T. Fan, and K. R. Chu, Phys. Rev. Lett. **89**, 268303 (2002).
[12] K. R. Chu, H. Y. Chen, C. L. Hung, T. H. Chang, L. R. Barnett, S. H. Chen, T. T. Yang, and D. Dialetis, IEEE Trans. Plasma Sci. **27**, 391 (1999).
[13] C. S. Kou, C. H. Chen, and T. J. Wu, Phys. Rev. E **57**, 7162 (1998).
[14] K. R. Chu and J. L. Hirshfield, Phys. Fluids **21**, 461 (1978).
[15] B. Boashash, *Time-Frequency Signal Analysis* (Halsted Press, New York, 1992).
[16] C. W. Peters, R. L. Jaynes, Y. Y. Lau, R. M. Gilgenbach, W. J. Williams, J. M. Hochman, W. E. Cohen, J. I. Rintamaki, D. E. Vollers, and T. A. Spencer, Phys. Rev. E **58**, 6880 (1998).
[17] O. Dumbrajs, T. Idehara, Y. Iwata, S. Mitsudo, I. Ogawa, and B. Piosczyk, Phys. Plasmas **10**, 1183 (2003).